

See discussions, stats, and author profiles for this publication at: <http://www.researchgate.net/publication/251567953>

# Cerebellar networks with basal ganglia: Feasibility for tracking cerebello-pallidal and subthalamo-cerebellar projections in the human brain

ARTICLE *in* EUROPEAN JOURNAL OF NEUROSCIENCE · JULY 2013

Impact Factor: 3.18 · DOI: 10.1111/ejn.12314 · Source: PubMed

CITATIONS

6

READS

105

6 AUTHORS, INCLUDING:



[Mathias Goldau](#)

University of Leipzig

13 PUBLICATIONS 33 CITATIONS

[SEE PROFILE](#)



[D. Y von Cramon](#)

Max Planck Institute for Metabolism Research

784 PUBLICATIONS 30,201 CITATIONS

[SEE PROFILE](#)



[Lars Timmermann](#)

University of Cologne

219 PUBLICATIONS 5,553 CITATIONS

[SEE PROFILE](#)



[Marc Tittgemeyer](#)

Max Planck Institute for Metabolism Research

139 PUBLICATIONS 1,777 CITATIONS

[SEE PROFILE](#)

# TECHNICAL SPOTLIGHT

## Cerebellar networks with basal ganglia: feasibility for tracking cerebello-pallidal and subthalamo-cerebellar projections in the human brain

Esther Annegret Pelzer,<sup>1,2</sup> Andreas Hintzen,<sup>1</sup> Mathias Goldau,<sup>1,3</sup> Detlev Yves von Cramon,<sup>1</sup> Lars Timmermann<sup>2</sup> and Marc Tittgemeyer<sup>1</sup>

<sup>1</sup>Max-Planck Institute for Neurological Research Cologne, Cologne, Germany

<sup>2</sup>Department of Neurology, University Hospital Cologne, Kerpener Strasse 62, Cologne 50937, Germany

<sup>3</sup>Institute of Informatics, University Leipzig, Leipzig, Germany

**Keywords:** basal ganglia, cerebellum, diffusion magnetic resonance imaging, segmentation protocol, tractography

### Abstract

Neuroanatomical studies using transneuronal virus tracers in macaque monkeys recently demonstrated that substantial interactions exist between basal ganglia and the cerebellum. To what extent these interactions are present in the human brain remains unclear; however, these connections are thought to provide an important framework for understanding cerebellar contributions to the manifestation of basal ganglia disorders, especially with respect to tremor genesis in movement disorders such as Parkinson's disease. Here, we tested the feasibility of assessing these connections *in vivo* and non-invasively in the human brain with diffusion magnetic resonance imaging and tractography. After developing a standardized protocol for manual segmentation of basal ganglia and cerebellar structures, masks for diffusion tractography were defined based on structural magnetic resonance images. We tested intra- and inter-observer stability and carried out tractography for dentato-pallidal and subthalamo-cerebellar projections. After robustly achieving connection probabilities per tract, the connectivity values and connectional fingerprints were calculated in a group of healthy volunteers. Probabilistic diffusion tractography was applicable to probe the inter-connection of the cerebellum and basal ganglia. Our data confirmed that dentato-thalamo-striato-pallidal and subthalamo-cerebellar connections also exist in the human brain at a level similar to those that were recently suggested by transneuronal tracing studies in non-human primates. Standardized segmentation protocols made these findings reproducible with high stability. We have demonstrated that diffusion tractography in humans *in vivo* is capable of revealing the structural bases of cerebellar networks with the basal ganglia. These findings support the role of the cerebellum as a satellite system of established cortico-basal ganglia networks in humans.

### Introduction

The traditional view that interactions between the cerebellum and basal ganglia occur mainly at the level of the cerebral cortex was recently challenged by studies applying transneuronal tracing with neurotropic viruses in non-human primates (Hoshi *et al.*, 2005; Bostan *et al.*, 2010). These studies revealed that an anatomical substrate exists for substantial interactions between the cerebellum and basal ganglia cortex loops (Bostan *et al.*, 2013), thereby suggesting that cerebellar contributions are implicated in motor as well as cognitive behaviour (Middleton & Strick, 2000) and also in the manifestation of prototypical basal ganglia disorders such as Parkinson's disease (PD). The very recent 'dimmer-switch' hypothesis of PD resting tremor stresses the pathophysiological importance of a strong inter-connectivity between cerebello-thalamo-cortical

circuits and the basal ganglia (Helmich *et al.*, 2012) by attributing the amplitude of PD tremor to activity in cerebellar pathways ('the dimmer'), and activity in the basal ganglia to the ON and OFF of the tremor ('the switch'). In fact, increasing evidence suggests that the cerebellum may have prominent roles in the pathophysiology of PD, as well as compensatory effects that may help to maintain better motor and non-motor functions (Wu & Hallett, 2013).

In humans, however, a systematic investigation of the neuroanatomical substrate for cerebellar involvement in these functions, mediated by the basal ganglia, is outstanding. Therefore, our investigation focused on the cerebellar network with basal ganglia in the human brain.

The classical view is that, in primates, efferents of cerebellar nuclei project through multiple subdivisions of the thalamus (Percheron *et al.*, 1996), which in turn project to widespread neocortical areas, including motor and premotor areas, as well as to the basal ganglia. Specifically for the ventral thalamic nucleus, overlaps between pallidal and cerebellar projection fields have been described

Correspondence: Esther Annegret Pelzer, <sup>2</sup>Department of Neurology, as above.  
E-mail: esther.pelzer@uk-koeln.de

Received 12 November 2012, revised 24 May 2013, accepted 20 June 2013

(Sakai *et al.*, 1996), suggesting potential contact between the basal ganglia and cerebellum on the thalamic level. Moreover, Ichinohe *et al.* (2000) showed projections from the lateral cerebellar nuclei (in the cat) to the dorso-lateral part of the striatum via the intra-laminar nuclei by using combined retrograde labelling and immunohistochemical methods.

Hoshi *et al.* (2005) extended these investigations on cerebellar projections to the pallidum in macaque monkeys. Using retrograde transneuronal virus transport, they were able to confirm previously described disynaptic projections from the deep cerebellar nuclei [mainly the dentate nucleus (DN)] to the dorsal striatum via predominantly intra-laminar, but also ventro-lateral, parts of the thalamus. Furthermore, they depicted trisynaptic projections to the external part of the pallidum, providing evidence for a direct subcortical communication, predominantly between the DN and basal ganglia. Based on these findings, Bostan *et al.* (2010) hypothesized that there is a multi-synaptic reciprocal inter-connection between basal ganglia and the cerebellum independent of the cerebral cortex. They found that the subthalamic nucleus (STN) gives rise to substantial disynaptic projections to cerebellar cortices (Crus II of lobule VIIA and VIIB) with pontine nuclei as relay stations.

All of these findings were achieved by tracing the transneuronal transport of neurotrophic viruses, mainly the rabies virus, in rats, cats or non-human primates. Whether and to what extent these specific connections between the basal ganglia and cerebellum exist in the human brain remains unclear.

In spite of novel developments in transneuronal tracing (e.g. Dum & Strick, 2012), the application of these techniques to the human brain remains elusive, due to the invasive nature of such methods. In contrast, recent developments in diffusion magnetic resonance imaging (dMRI) and diffusion tractography may allow for non-invasive and *in vivo* studies of the anatomical substrate of basal ganglia systems (Draganski *et al.*, 2008) and cerebellar circuits (Granziera *et al.*, 2009) in humans; even if this application has some limitations (Jbabdi & Johansen-Berg, 2011) and the validity of diffusion tractography remains difficult with respect to showing a congruence with true axonal fibre pathways (e.g. Seehaus *et al.*, 2013), it can provide supporting evidence and thus foster our understanding of the variability of *in vivo* connectivity in rather large brain samples, even in a clinical setting.

Here, we strived to test the hypotheses that substantial interactions, at least on the level shown in animal studies, also exist between the cerebellum and basal ganglia in the human brain, and that it is feasible to resolve these connections by diffusion tractography.

## Materials and methods

### Magnetic resonance imaging data acquisition

Twelve healthy native German volunteers [right-handed, predominantly female ( $n = 10$ ), mean age 26.5 (SD 4.4) years] were analysed. All subjects provided written consent as per the declaration of Helsinki and the approval of the local ethics committee. High-resolution  $T_1$ - and  $T_2$ -weighted images were acquired using a Siemens 3T Trio scanner (12-channel array head coil; maximum gradient strength 40 mT/m) with a whole-brain field of view ( $T_1$ -weighted: MDEFT3D; time of repetition, 1930 ms; time to inversion, 650 ms; echo time, 5.8 ms; 128 sagittal slices; resolution,  $1 \times 1 \times 1.25 \text{ mm}^3$ ; flip angle,  $18^\circ$ ;  $T_2$ -weighted: rapid acquisition with relaxation enhancement; time of repetition, 3200 ms; echo time, 458 ms; 176 sagittal slices; resolution,  $1 \times 1 \times 1 \text{ mm}^3$ ). Further-

more, diffusion-weighted data (dMRI) were collected using echo-planar imaging with double-spin echo preparation (Reese *et al.*, 2003; twice-refocused spin echo planar imaging; time of repetition, 9000 ms; echo time, 87 ms; 72 axial slices; resolution,  $1.7 \times 1.7 \times 1.7 \text{ mm}^3$ ). Diffusion weighting was isotropically distributed along 60 directions with a  $b$ -value of  $1000 \text{ s/mm}^2$ . The high angular resolution of the diffusion weighting directions improves the robustness of probability density estimation by increasing the signal-to-noise ratio and reducing directional bias. Seven images without diffusion weighting were acquired at the beginning and after each block of 10 diffusion-weighted images as an anatomical reference for motion correction. To further increase the signal-to-noise ratio, we acquired three consecutive scans, which were subsequently averaged together. The entire data acquisition protocol lasted approximately 45 min. The dMRI data were acquired after the  $T_1$ - and  $T_2$ -weighted images in the same scanner reference system.

Of these 12 subjects, datasets of three subjects were randomly chosen to test the inter-observer [two observers (E.A.P. and A.H.) independently] and intra-observer reliability of masks and feasibility of tracking the dentato-pallidal and subthalamo-cerebellar pathways. The dentato-pallidal pathway was then analysed in all 12 subjects.

In the analysis of the subthalamo-cerebellar connections, however, it turned out that, due to different head sizes, the cerebellum was initially not optimally kept in all dMRI acquisitions of every subject. To ensure completeness of the cerebellar cortex, 12 further subjects were recruited and the dMRI protocol was expanded to 90 axial slices; all other magnetic resonance imaging parameters were identical to the protocol described above.

### Image preprocessing

All preprocessing steps were carried out using programs from the FSL software package (version 4.1.9; FMRIB Software Library, University of Oxford, <http://fsl.fmrib.ox.ac.uk/fsl/fslview/>). In a first step, the  $T_1$ -weighted images were skull-stripped and reoriented to the sagittal plane through anterior and posterior commissures. Upon reorientation, these  $T_1$  images were then registered to the Montreal Neurological Institute (MNI)-152 1 mm standard brain by using an affine registration (Jenkinson & Smith, 2001). Later, the respective registration matrices also led to co-registration of the  $T_2$ -weighted images to standard space.

Motion correction of diffusion-weighted images was applied to all images using seven-parameter global rescale registration (Jenkinson *et al.*, 2002). All baseline  $b_0$  images were aligned to a reference  $b_0$  image and the resulting linear transformation matrices were then applied to the diffusion-weighted images following each baseline  $b_0$  image. The gradient direction for each volume was corrected using rotation parameters. The three scan repetitions were then averaged to improve the signal-to-noise ratio.

Before starting tractography, the diffusion images together with structural images were linearly co-registered (Jenkinson & Smith, 2001) to the MNI-152 1 mm isotropic brain. This linear transformation was then used to initialize a non-linear normalization procedure (Andersson *et al.*, 2007) to the MNI reference space, and was inverted for tractography.

### Tractography

The FDT toolbox (<http://www.fmrib.ox.ac.uk/fsl/fdt/>), as implemented in the FSL software, was applied to probabilistic diffusion tractography. FDT repetitively samples from the distributions on

voxel-wise principal diffusion directions, each time computing a streamline through these local samples to generate a probabilistic streamline. By taking many such samples, FDT is able to build upon the posterior distribution on the streamline location or the connectivity distribution (Behrens *et al.*, 2007). The local diffusion directions are calculated using the program *bedpostx*, which allows modelling of multiple fibre orientations per voxel; the program *probtrackx* then involves generating connectivity distributions from user-specified seed voxels (Behrens *et al.*, 2003a). For each subject and seed region, identical numbers of program parameters were chosen, namely: number of samples,  $P = 5000$ ; number of steps,  $P = 2000$ ; step length, 0.5 mm; curvature threshold,  $c = 0.2$  (corresponding to a minimum angle of approximately  $\pm 80$  degrees), see also [http://fsl.fmrib.ox.ac.uk/fsl/fsl4.0/fdt/fdt\\_probtrackx.html](http://fsl.fmrib.ox.ac.uk/fsl/fsl4.0/fdt/fdt_probtrackx.html).

Tractography was performed for each subject individually in his/her native space. The resulting connectivity maps were then warped into a standard space (using the MNI 1 mm isotropic brain as a reference) for cross-subject averaging and comparison. To create seed masks for each subject, MNI coordinates were normalized to each subject's native space, using the inverse of the normalization parameters. All resulting images were visually inspected to ensure that normalization was successful and that each image was acceptable for analysis (e.g. in the correct orientation and not distorted).

Tractography results were visualized with the 'fibre-stippling' method (Goldau *et al.*, 2011) from the tool OpenWalnut (Image and Signal Processing Group, University of Leipzig, Germany; <http://www.openwalnut.org>).

### Connectivity measure

Considering all fibres originating in a given seed region  $S$ , its structural connectivity with a given target region  $T$  can be defined in terms of the proportion of those fibres that intersect  $T$  while running within the brain white matter, yielding a number in the interval between 0 (no fibres intersect  $T$ ) and 1 (all fibres starting in  $S$  reach  $T$ ; Kaden *et al.*, 2007). This quantity gives no information about the absolute number of connections between two regions, but reflects the degree of connectedness or relative connection density. It can be considered as a measure of the likelihood of a connection in the sense that it can be interpreted as the frequency at which one would reach  $T$  by randomly seeding a fibre starting within  $S$ . In our framework, the notions of anatomical connection strength and anatomical connection likelihood are therefore interchangeable [for a more detailed discussion of this issue, cf. Stephan *et al.* (2009)].

One should note, however, that this connectivity metric might differ depending on whether  $S$  or  $T$  is chosen as the seed region for tractography (noting that this does not reflect the directionality of synaptic transmission along the pathways). For any given (probabilistic) measure  $\varphi_{ST}^*$  of anatomical connectivity, one can remove this dependency on the seed region by computing the connectivity metric using each region as a seed region once and then averaging the result. Following this procedure, anatomical connectivity was estimated in each subject for all of the connections. The subject-specific anatomical connection probabilities were then averaged across subjects, individually per observer.

Generally, these values will describe a probability density, e.g. the probability of a streamline from a seed region to reach a target region. Because these measures are densities, their absolute values depend on their units of measurement (e.g. per voxel). This dependency was resolved by working with the relative probabilities on  $n$  connections.

$$\varphi_{ST} = \frac{\varphi_{ST}^*}{\sum_{ST} \varphi_{ST}^*}.$$

This ensures that  $\sum \varphi_{ST} = 1$  and furnishes a measure of anatomical strength for any one connection, relative to all others.

### Outlining of masks

After proof of data quality (in terms of completeness, field homogeneity, absence of artefacts, sufficient signal-to-noise ratio), masks were outlined on  $T_1$ - $T_2$ -weighted images as described above by using *fslview* (<http://www.fmrib.ox.ac.uk/fsl/fslview>). Before mask drawing, both observers (E.A.P. and A.H.) attended an intensive traineeship with an anatomical expert (J. K. Mai, University Hospital Düsseldorf, Germany) as well as on the basis of anatomical and neurosurgical atlases (Schaltenbrand & Wahren, 1977; Mai *et al.*, 1997; Schmahmann *et al.*, 1999; Morel, 2007; Naidich *et al.*, 2009). Mask location was chosen upon comparison of these atlases and both observers developed a common segmentation protocol in order to obtain a distinguished anatomical reliability and inter-observer stability.

To enhance the intra-observer stability, every mask was outlined three times per region by both observers. The following protocol has been applied (see Fig. 1).

1. Definition of the mask to start tractography from the DN (the main source of deep cerebellar nuclei projections; Hoshi *et al.*, 2005). The thalamus, dorsal striatum (caudate nucleus; putamen) and pallidum (internal and external part) were chosen as waypoint and/or target masks. Regarding the thalamus, we chose to not further subdivide the mask but to use an outline for the whole thalamus (excluding the lateral geniculate nucleus). Boundaries between thalamic nuclei that can be visualized histologically (Morel, 2007) are not reliably distinguishable in magnetic resonance imaging, even when using a contrast-optimized protocol (Magnotta *et al.*, 2000). Approaches to automatically segmenting the thalamus based on dMRI and cortical connectivity information have been shown to be stable (Behrens *et al.*, 2003b; Johansen-Berg *et al.*, 2005), but such approaches have not yet been proven valid when subcortical connectivity is also considered.

2. Definition of the STN as the seed mask for tractography and the cerebellar cortex as the target mask.

After a stable outlining procedure, segmentation was performed on all subjects with the following segmentation protocol (see Fig. 1).

### Segmentation protocol

#### Dentate nucleus

In the axial plane of  $T_2$ -weighted images, the DN emerges with two parts: a more hyperdense medial part, where the efferent fibres leave, and the more hypodense lateral part with reaching afferences (Naidich *et al.*, 2009; both parts were considered for segmentation). Adjacent structures that medially (i.e. the fourth ventricle) or rostromedially (i.e. the nuclei fastigii) border the DN were clearly visible and were thus excluded from the mask. Conversely, the interposed nucleus was hardly visible and thus was included in the mask.

#### Thalamus

Segmentation was carried out based on  $T_1$ -weighted images in the coronal plane, with the exception of the limit to posteriorly located structures (hippocampal area and tail of the caudate nucleus), where

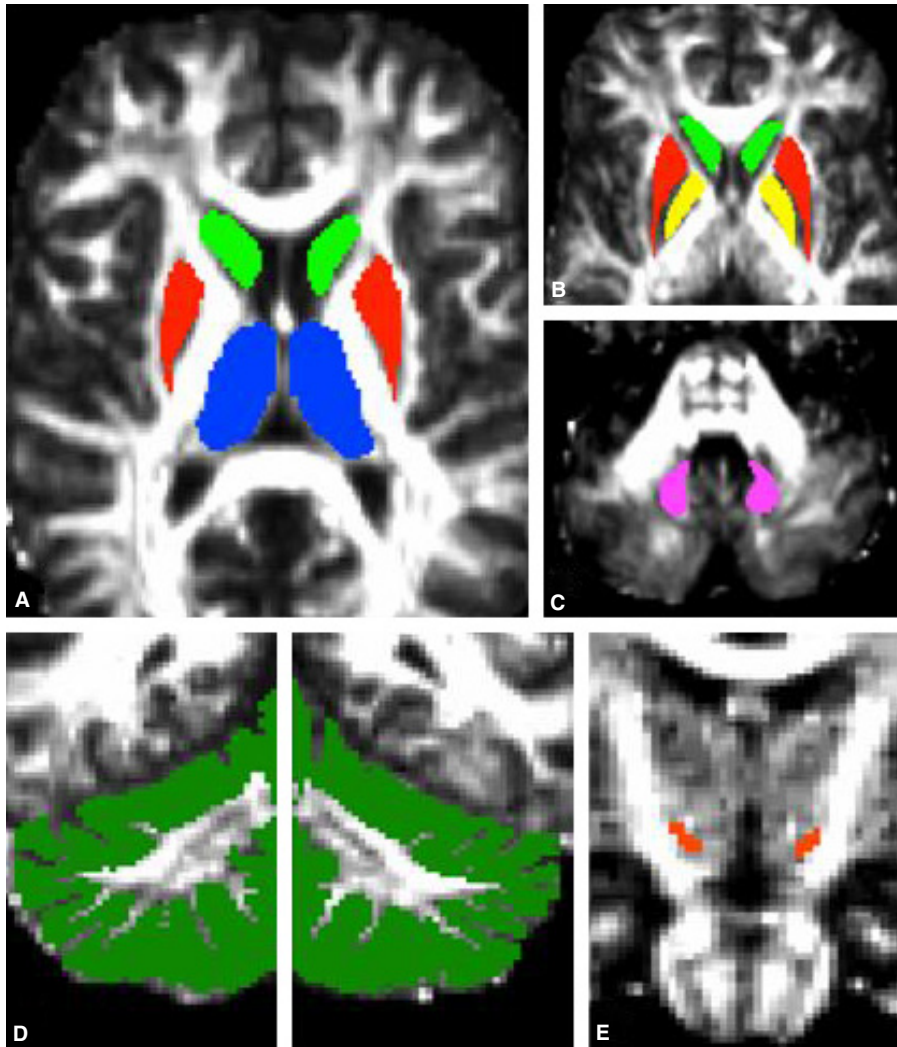


FIG. 1. Sketch of manual segmentation outlined on corresponding maps of fractional anisotropy. Masks of DNs are depicted in the axial plane: (A) thalamus (blue), putamen (red) and caudate nucleus (bright green); (B) putamen (red), caudate nucleus (bright green) and pallidum (yellow); and (C) DN (magenta). Masks of subthalamic projections are shown in the coronal plane: (D) cerebellum (green); and (E) STN (red).

the mask was carefully controlled in the axial plane. Outlining the thalamus was performed in an anterior-to-posterior course.

The medial boundary of the anterior thalamus was defined by the stria terminalis, whereas the internal capsule defined a lateral and ventro-lateral limit. The ventro-medial border was outlined at the appearance of the inferior thalamic peduncle. The lateral ventricle and ventral caudate nucleus defined a dorsal border. Furthermore, the third ventricle defined the medial, whereas the lateral ventricle defined the medio-dorsal boundary. As the dorsal border, we accounted for the stria terminalis and dorso-laterally the caudate nucleus and genu of the internal capsule. Ventro-medially, the hypothalamic area limited the thalamus mask; the red nucleus was used as a reference to identify the ventral boundary in the posterior course.

The appearance of the medial geniculate nucleus defined the starting point for the segmentation in the posterior thalamus; here, the medial geniculate nucleus also had to be included in the mask. The lateral geniculate nucleus was excluded. Medially and dorso-medially, the lateral ventricle and dorso-laterally the caudate nucleus constituted the border. The pretectal area provided the ventral boundary. The lateral boundary was defined by the posterior limb of

the internal capsule, which was additionally confirmed by overlying a diffusion tensor based eigenvector map (cf. Wiegell *et al.*, 2003).

The ventro-medial limit was the epithalamus and subhabenula nucleus; the ventro-lateral limit was the triangular area (area of Wernicke) and optic radiation, as well as the lateral geniculate nucleus. In the posterior course, the thalamus shrunk more and more, with the lateral and third ventricle providing a dorsal and medial boundary, and the brachium of the superior colliculus providing a ventral boundary. The stria terminalis and the tail of the caudate nucleus limited the thalamus laterally until it disappeared.

#### *Dorsal striatum*

After locating its ventral border in the coronal plane at the dorso-lateral point of the anterior commissure at the level of the inter-hemispheric fibre crossing, the mask of the putamen was outlined on T<sub>1</sub>-weighted images in the axial plane. Here, every structure ventral to the anterior commissure and the striatal fundus region was excluded from the mask. On the lateral side, the external capsule and medially the anterior limb of the internal capsule were chosen as

borders. Posteriorly, the posterior limb of the internal capsule defined a boundary of the putamen mask. In a dorsal direction, outlining was continued with regard to the boundary to the external capsule. After segmentation, mask positioning was confirmed in coronal slices.

The mask for the head of the caudate nucleus was outlined on T<sub>1</sub>-weighted images in the axial plane. The caudate tail was not included in the mask because of its small size, uncertain boundary and observer instabilities in tracing. At the largest diameter of the anterior commissure, the ventral boundary of the caudate head was defined, delimiting it here from the accumbens nucleus. On the medial side, the lateral ventricle and on the lateral side the anterior limb of the internal capsule were chosen as delimiter; here, the slightly hypodense lateral branches to the putamen 'smudged' into the internal capsule and were neglected. Finally, the stria terminalis and subcallosal stratum bordered the caudate nucleus dorsally. Mask positioning was confirmed in coronal slices.

### Pallidum

The mask for the pallidum was outlined in the coronal plane of T<sub>1</sub>-weighted images. Segments of the anterior commissure, the ventral pallidum and internal medullary lamina bordered the pallidum ventrally next to the nucleus basalis Meynert and ansa lenticularis. Whereas the genu and posterior limb of the internal capsule limited

the mask on the medial side, the anterior limb of the internal capsule limited the dorso-medial side. Laterally, the thin lateral medullary lamina formed the boundary between the pallidum and putamen. In the coronal plane, the pallidum appeared with a triangular shape and looked much less hypodense than the putamen. In the dorsal direction, it successively disappeared. Location of the segmented mask was confirmed in the axial plane; in particular, the lateral bordering of the putamen, predominantly to the external medullary lamina, was controlled.

### Subthalamic nucleus

The mask for the STN was outlined on T<sub>2</sub>-weighted images in the coronal plane. Initially the red nucleus was localized. In the anterior direction, the red nucleus disappeared progressively and the hypodense and 'lens-like' STN appeared dorso-laterally on the top of the substantia nigra. The main axis of the STN (compared with a fictive horizontal axis) was found to be tilted upwards at approximately 45°. As the ventro-medial boundary of the STN, the substantia nigra was delineated and successively dorso-laterally the zona incerta, dorso-medially the fields of Forel (H1 and H2), and laterally the posterior limb of the internal capsule. The STN was outlined in the anterior direction until the substantia nigra disappeared. In the anterior course, the STN appeared more and more medially until it became

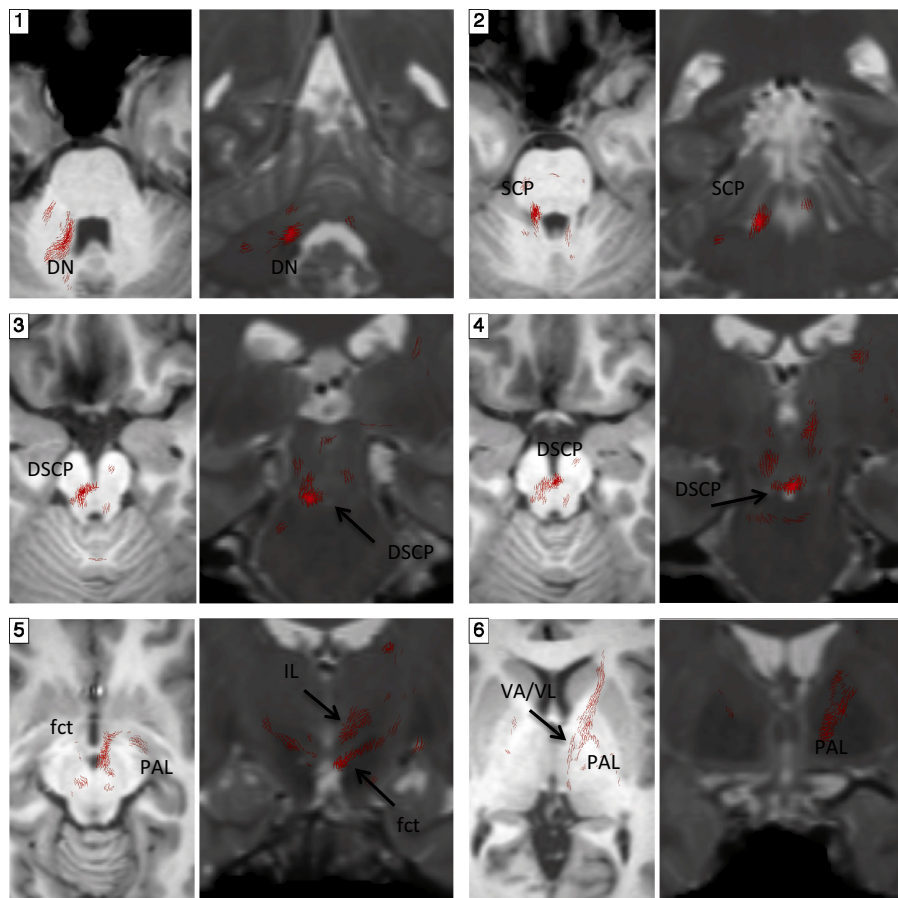


FIG. 2. Dentato-thalamo-striato-pallidal connections at an example of right dentate projections in axial (left) and coronal (right) slices. Fibre course from the right DN (1) passing the right superior cerebellar peduncle (SCP) (2), crossing to the contralateral side via the decussation of the superior cerebellar peduncle (DSCP) at the beginning (3) and at the crossing (4). The ascendancy towards the thalamus occurs via the cerebello-thalamic tract (fct), then pallidal fibre projections leave the tract to putatively enter the intra-laminar nuclei (IL) (5) with egression of the thalamus at the level of the ventro-lateral/ventro-anterior (VA/VL) (6) nuclei; here fibre trajectories yield to the pallidum (PAL) on the left side (6).

invisible when the mammillary bodies appeared. The position of the mask was confirmed in the sagittal as well as in the axial plane.

### Cerebellar cortex

The mask of the cerebellar cortex was traced on T<sub>1</sub>-weighted images in the coronal plane. The subdivision of the cerebellar lobules was chosen in analogy to the nomenclature of Larsell *et al.* (1972). No distinction in nomenclature was made between the vermis and hemispheres. Parts of the anterior lobe (III, IV and V), the superior posterior lobe (VI and Crus I of VIIA) and parts of the inferior posterior lobe (Crus II of VIIA, VIIB, VIII and IX) were included in segmentation in order to use the localization of the neuronal tracer study of Bostan *et al.* (2010). In the anterior lobe, lobules I/II appeared as a single structure and lay against the superior medullary vellum (these anterior boundaries were excluded from outlining). The cerebellar peduncles and cerebellar central white matter medially limited the cerebellar cortex, which had here a typical hypodense appearance with its folia as the surface structure. The skull provided the lateral border and the posterior boundary structure of the inferior posterior lobe to lobule X was the postero-lateral fissure (lobule X was not included in the mask). Positioning of the segmented mask was finally confirmed in axial slices.

## Results

We initially examined the cerebello-pallidal pathway, and four 'relay stations' for comparison with the results from the transneuronal tracer studies [according to Hoshi *et al.* (2005)] were considered: (i) dentato-thalamic projections, (ii) dentato-thalamo-putaminal projections, (iii) dentato-thalamo-caudatal projections, and (iv) dentato-thalamo-striato-pallidal projections. Furthermore, projections from the STN to the cerebellar cortex (Bostan *et al.*, 2010) were analysed.

Diffusion tractography was found to be applicable to probe the inter-connection of the cerebellum with the basal ganglia, and we were able to trace the dentato-pallidal (Fig. 2) as well as the subthalamo-cerebellar (Fig. 3) pathway. Intra-observer reliability was high for all subjects and masks, yet significant differences in voxel quantities between observers were found for the left putamen, right thalamic nucleus and right DN (all masks,  $P < 0.05$ ). Also, the number of overlapping voxels between both observers was reasonably high (DN 83% and STN 75%) but the general size of the mask revealed a significant influence on the stability of tractography results.

In addition to the relative quantification of connectivity between the seed and target areas (see below), diffusion tractography allowed us to trace the pathways. It is noteworthy that we found both

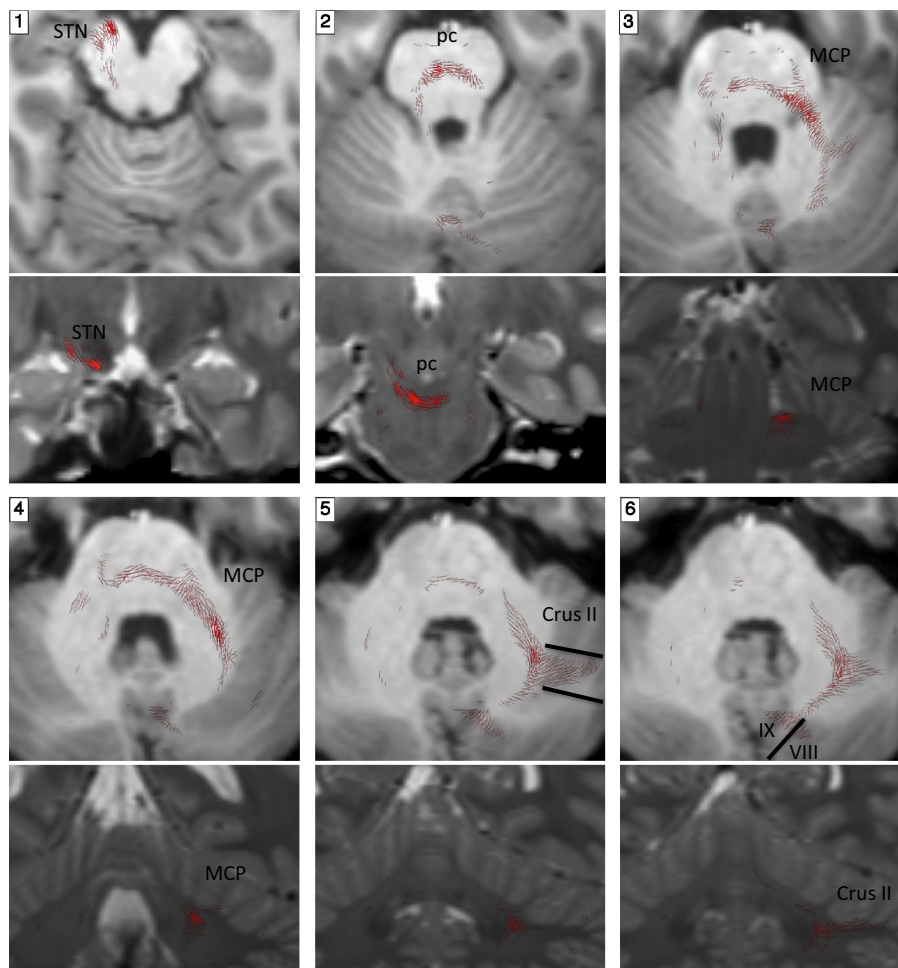


FIG. 3. Subthalamo-cerebellar connections on axial (superior) and coronal (inferior) slices at an example of the left STN. After tracing from the left STN (1), the tract crosses to the contralateral side at the level of the ponto-cerebellar fibres crossing (pc) (2) to reach the middle cerebral peduncle (MCP) (3); by passing through the MCP (4), the tract enters the cerebellar cortex (5) towards crus II (5) and lobules VIII and IX (6).

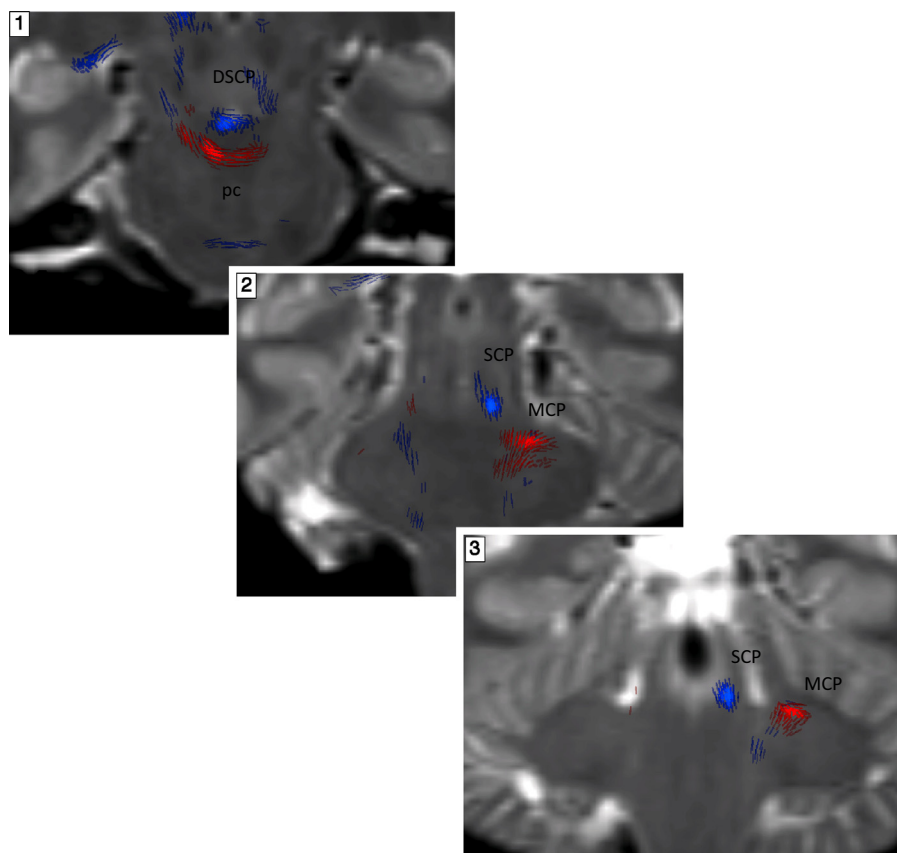


FIG. 4. Fibre crossing in the brainstem. (1) Fibre crossing of the dentate-thalamo-striato-pallidal connections on coronal slices at the level of the decussation of the superior cerebellar peduncle (DSCP; blue) and subthalamo-cerebellar connections at the ponto-cerebellar fibre crossing (pc; red). (2 and 3) Pathways enter into the cerebellum at different levels, either via the superior cerebellar peduncle (SCP; blue) or middle cerebellar peduncle (MCP; red). [Color version of figure available online].

pathways to be entering the cerebellum at different levels at the pons (Fig. 4), thereby pointing towards a different functional role of these fibres in the interaction with the basal ganglia.

#### Dentato-thalamo-striato-pallidal connections

Projections from the DN reached the contralateral hemisphere by passing intra-laminar and ventral parts of the thalamus (Fig. 2), confirming the data in non-human primates. In the feasibility test, connectivity values were highly reproducible within and between both observers for all target areas of the DN (Table 1). Furthermore, connectivity between DN and the thalamus was found to be massive, with an average connection probability of  $\phi = 68\%$  (SE 5.8%). We also found a slightly stronger connectivity from the DN

TABLE 1. Inter-observer comparison of connectivity values of dentate projections to different target regions

DN connectivity ( $\phi$ ) with target areas (%)	Pallidum	Caudate nucleus	Putamen	Thalamus
Observer 1	11 (SE 1.57)	11 (SE 0.77)	9 (SE 2.10)	68 (SE 4.24)
Observer 2	10 (SE 2.54)	12 (SE 2.17)	9 (SE 2.66)	68 (SE 7.35)

Results were highly similar between both observers, although SEs differed between observers 1 and 2 with highest SE values for the thalamus, due to the non-specific labelling of the thalamus as target mask (see Materials and methods).

to the caudate nucleus,  $\phi = 12\%$  (SE 1.5%), than to the putamen,  $\phi = 9\%$  (SE 2.4%), and pallidum,  $\phi = 11\%$  (SE 2.0%; see Fig. 5).

After feasibility testing, we analysed the dentato-pallidal connections in 12 healthy subjects. No statistical difference was found between the left and right mask size of the DN, putamen, caudate nucleus and thalamus; however, a significant difference in voxel size was found in the comparison of the left and right pallidum ( $P < 0.05$ ). The tractography and calculation of connectivity values were highly reproducible in the left and right hemisphere, very similar to the distribution of connectivity values in our feasibility study.

Connectivity between the DN and thalamus was found to be massive, with an average connection probability of  $\phi = 79\%$  (SE 3.67%). We found a stronger connectivity from the DN to the caudate nucleus,  $\phi = 10\%$  (SE 0.76%), than to the putamen,  $\phi = 5\%$  (SE 0.01%), and pallidum,  $\phi = 5\%$  (SE 0.42%). Statistically, in all 12 subjects there was no difference in the connectivity values of the dentate projections for the left and right side of the pallidum, caudate nucleus, putamen, and thalamus ( $P > 0.05$ ).

#### Subthalamo-cerebellar connections

Connections between the STN and cerebellar cortex (Crus II; lobule VII b; Fig. 3) could be clearly confirmed, in agreement with the findings of Bostan *et al.* (2010). In addition, we also found connections to lobules VIII and IX. The fibre crossing to the contralateral side at the level of the pons was well resolved, and the entrance of fibres into the cerebellum was observed at the level of the middle cerebellar

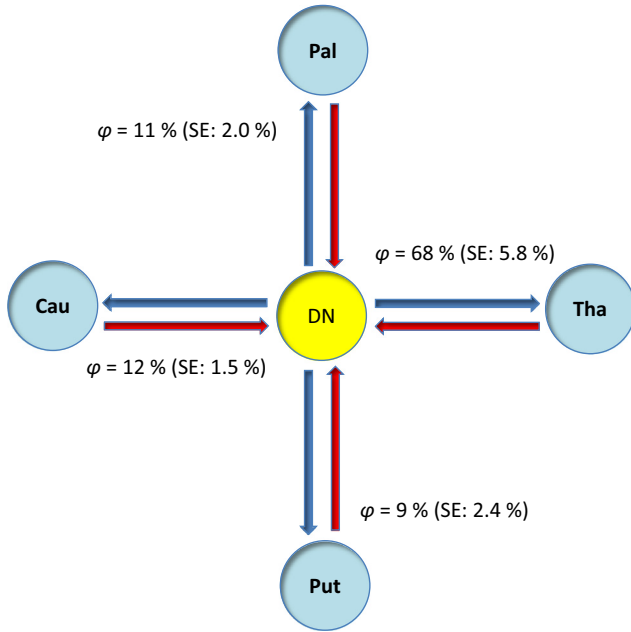


FIG. 5. Connectivity probabilities for dentato-thalamo-striato-pallidal connections of the first experiment. Because of high intra- and inter-observer stability, results were not further subdivided into findings for observers 1 and 2. Connectivity values to the thalamus were high at  $\phi = 68\%$  (for more details see Table 1). Cau, Caudate nucleus; Pal, pallidum; Put, putamen; Tha, Thalamus.

peduncle. In the feasibility test, STN connectivity was stronger than dentato-pallidal connectivity in all three subjects, also showing significantly ( $P < 0.05$ ) higher inter-individual differences:  $\phi_{\text{sub},1} = 41\%$  (SE 0.4%),  $\phi_{\text{sub},2} = 36\%$  (SE 0.6%), and  $\phi_{\text{sub},3} = 22\%$  (SE 1.0%); see also Fig. 6).

After feasibility testing, we analysed the connectivity values for the subthalamo-cerebellar connections. These were not as stable as the dentato-pallidal connections, yet there were no significant differences between the subjects. The median of the connectivity values

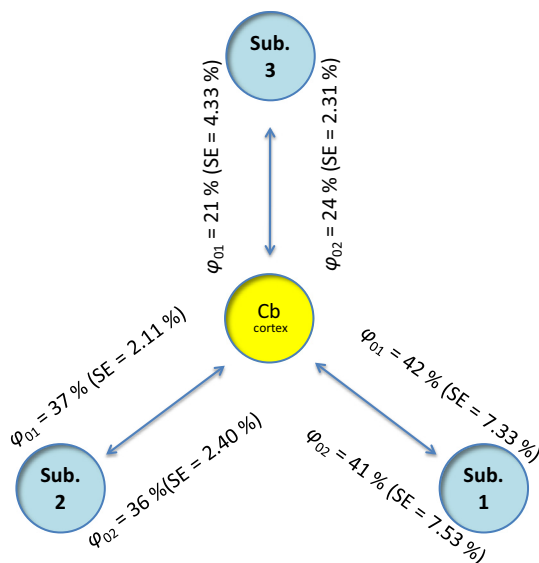


FIG. 6. Connectivity probabilities for subthalamo-cerebellar connections for the first experiment. Intra-subject connection probabilities were stable between both observers although inter-subject results diverged. Cb, cerebellum; Sub, subthalamic nucleus.

for the subthalamo-cerebellar connection was stronger than in the feasibility study, with  $\phi = 50\%$ .

## Discussion

To date, diffusion tractography provides the only method of probing anatomical connection probabilities *in vivo* and non-invasively. Here, we tested the feasibility of investigating anatomical connections by diffusion tractography between the cerebellum and basal ganglia. Moreover, we proposed a segmentation protocol with the objective of achieving stable and reliable connectivity measures between these brain regions. Thereby, for the first time, we have found that subtle connections between the basal ganglia and cerebellum can also be traced in the human brain, *in vivo* and non-invasively. In particular, we were able to anatomically delineate connections from the DN to basal ganglia structures as well as from the STN to the cerebellar cortex using probabilistic tractography. These results are in accordance with the findings of Hoshi *et al.* (2005) from anatomical tracing studies in non-human primates. Also, in agreement with the results of Hoshi *et al.* (2005), connectivity values to the dorsal striatum and pallidum were low. We found a slightly stronger connectivity from the DN to the caudate nucleus than to the putamen and pallidum (Fig. 5).

Connectivity between the STN and cerebellar cortex was significantly higher ( $P < 0.03$ ) in all subjects than connections from the DN to the basal ganglia, indicating a greater functional significance of the first fibre connection. These connectivity values showed a rather high inter-individual variability, although the segmentation protocol of STN masks led to high congruence in the voxel analysis of the STN size between the observers. There may be two reasons generating this variability. The boundary of the seed masks to surrounding structures importantly influences the stability of connection probabilities. Whereas the boundary of the DN was seemingly clearly definable from surrounding structures in  $T_2$ -weighted images, thus leading to a large congruence between observers, the STN has a small size and is actually difficult to delineate from surrounding structures due to disadvantageous contrast properties. Although the volume measures that we found for the STN were similar to the voxel size of recently published studies (Yelnik *et al.*, 2007; Massey *et al.*, 2012), delineating the STN from magnetic resonance imaging scans is a matter of intensive discussion, which may be due to differences in STN subfield organization (Keuken *et al.*, 2012) or inter-individual variability in iron accumulation of the STN leading to differences in magnetic susceptibility (Schäfer *et al.*, 2011; Massey *et al.*, 2012). Therefore, although the presented segmentation protocol might reflect the borders of the STN, implementation of additional magnetic resonance imaging protocols such as quantitative susceptibility mapping (like R2\*) might be necessary, together with multi-modal segmentation procedures of the STN (Bilgic *et al.*, 2012).

Moreover, probabilistic tractography is inherently distance dependent (Behrens *et al.*, 2007), i.e. the further that target points are away from the starting point of a tractogram, the lower the resulting probabilities. Here, probabilistic tractography was able to reproduce anatomical findings, but led to small connectivity values especially for more distant brain areas. This might reflect a potential signal loss due to fibre crossing in the brainstem. By correcting probability values for distance, we obtained much higher connectivity values, but 'absolute' connectivity values were distorted. In order to be able to compare the absolute connectivity values of different subjects, we continued to work with low raw connectivity values. In general, this procedure was validated (Dyrby *et al.*, 2007; Seehaus *et al.*, 2013), but long anatomical distances, fibre crossings and the performance

of tractography through high isotropic areas with potential signal loss still burden the tracing of long-range connections. The potential interference in the investigation of basal ganglia–cerebellar interactions has to be systematically elucidated in further studies. An important role of the cerebellum in PD, however, has been highlighted recently (Wu & Hallett, 2013), and the investigation of structural changes in basal ganglia–cerebellar interactions in the human is part of on-going research.

## Acknowledgements

The authors wish to thank Jürgen K. Mai (Institute of Anatomy, University of Düsseldorf) for insightful discussions with respect to mask preparation and the anatomical delineations of basal ganglia and cerebellar structures. This work was supported by the funding of the German Research Foundation (DFG) in the Clinical Research Group 219 (KFO 219).

## Abbreviations

dMRI, diffusion magnetic resonance imaging; DN, dentate nucleus; MDI, Montreal Neurological Institute; PD, Parkinson's disease; STN, subthalamic nucleus.

## References

- Andersson, J.L.R., Jenkinson, M., Smith, S. & Andersson, J. (2007) Non-linear registration, aka spatial normalization: FMRIB technical report TR07JA2. *FMRIB Analysis Group of the University of Oxford*.
- Behrens, T., Woolrich, M., Jenkinson, M., Johansen Berg, H., Nunes, R., Clare, S., Matthews, P., Brady, J. & Smith, S. (2003a) Characterization and propagation of uncertainty in diffusion-weighted MR imaging. *Magn. Reson. Med.*, **50**, 1077–1088.
- Behrens, T.E.J., Johansen-Berg, H., Woolrich, M.W., Smith, S.M., Wheeler-Kingshott, C.A.M., Boulby, P.A., Barker, G.J., Sillery, E.L., Sheehan, K., Ciccarelli, O., Thompson, A.J., Brady, J.M. & Matthews, P.M. (2003b) Non-invasive mapping of connections between human thalamus and cortex using diffusion imaging. *Nat. Neurosci.*, **6**, 750–757.
- Behrens, T.E.J., Berg, H.J., Jbabdi, S., Rushworth, M.F.S. & Woolrich, M.W. (2007) Probabilistic diffusion tractography with multiple fibre orientations: what can we gain? *NeuroImage*, **34**, 144–155.
- Bilgic, B., Pfefferbaum, A., Rohlfing, T., Sullivan, E.V. & Adalsteinsson, E. (2012) MRI estimates of brain iron concentration in normal aging using quantitative susceptibility mapping. *NeuroImage*, **59**, 2625–2635.
- Bostan, A.C., Dum, R.P. & Strick, P.L. (2010) The basal ganglia communicate with the cerebellum. *Proc. Natl. Acad. Sci. USA*, **107**, 8452–8456.
- Bostan, A.C., Dum, R.P. & Strick, P.L. (2013) Cerebellar networks with the cerebral cortex and basal ganglia. *Trends Cogn. Sci.*, **17**, 241–254.
- Draganski, B., Kherif, F., Klöppel, S., Cook, P.A., Alexander, D.C., Parker, G.J.M., Deichmann, R., Ashburner, J. & Frackowiak, R.S.J. (2008) Evidence for segregated and integrative connectivity patterns in the human basal ganglia. *J. Neurosci.*, **28**, 7143–7152.
- Dum, R.P. & Strick, P.L. (2012) Transneuronal tracing with neurotropic viruses reveals network macroarchitecture. *Curr. Opin. Neurobiol.*, **23**, 245–249.
- Dyrby, T.B., Sogaard, L.V., Parker, G.J., Alexander, D.C., Lind, N.M., Baare, W.F.C., Hay-Schmidt, A., Eriksen, N., Pakkenberg, B., Paulson, O.B. & Jelsing, J. (2007) Validation of *in vitro* probabilistic tractography. *NeuroImage*, **37**, 1267–1277.
- Goldau, M., Wiebel, A., Gorbach, N.S., Melzer, C., Hlawitschka, M., Scheuermann, G. & Tittgemeyer, M. (2011) Fiber stippling: an illustrative rendering for probabilistic diffusion tractography. In Goldau, M., Melzer, C., Scheuermann, G. & Tittgemeyer, M. (Eds), *IEEE Proceedings BioVis 2011*. Providence, Rhode Island, USA, pp. 23–30.
- Granziera, C., Schmahmann, J.D., Hadjikhani, N., Meyer, H., Meuli, R., Wedeen, V. & Krueger, G. (2009) Diffusion spectrum imaging shows the structural basis of functional cerebellar circuits in the human cerebellum *in vivo*. *PLoS One*, **4**, e5101.
- Helmich, R.C., Hallett, M., Deuschl, G., Toni, I. & Bloem, B.R. (2012) Cerebral causes and consequences of parkinsonian resting tremor: a tale of two circuits? *Brain*, **135**, 3206–3226.
- Hoshi, E., Tremblay, L., Féger, J., Carras, P.L. & Strick, P.L. (2005) The cerebellum communicates with the basal ganglia. *Nat. Neurosci.*, **8**, 1491–1493.
- Ichinohe, N., Mori, F. & Shoumura, K. (2000) A di-synaptic projection from the lateral cerebellar nucleus to the laterodorsal part of the striatum via the central lateral nucleus of the thalamus in the rat. *Brain Res.*, **880**, 191–197.
- Jbabdi, S. & Johansen-Berg, H. (2011) Tractography: where do we go from here? *Brain Connectivity*, **1**, 169–183.
- Jenkinson, M. & Smith, S. (2001) A global optimisation method for robust affine registration of brain images. *Med. Image Anal.*, **5**, 143–156.
- Jenkinson, M., Bannister, P., Brady, M. & Smith, S.M. (2002) Improved optimization for the robust and accurate linear registration and motion correction of brain images. *NeuroImage*, **17**, 825–841.
- Johansen-Berg, H., Behrens, T.E.J., Sillery, E., Ciccarelli, O., Thompson, A.J., Smith, S.M. & Matthews, P.M. (2005) Functional-anatomical validation and individual variation of diffusion tractography-based segmentation of the human thalamus. *Cereb. Cortex*, **15**, 31–39.
- Kaden, E., Knösche, T.R. & Anwander, A. (2007) Parametric spherical deconvolution: inferring anatomical connectivity using diffusion MR imaging. *NeuroImage*, **37**, 474–488.
- Keuken, M.C., Uylings, H.B.M., Geyer, S., Schäfer, A., Turner, R.S. & Forstmann, B.U. (2012) Are there three subdivisions in the primate subthalamic nucleus? *Front. Neuroanat.*, **6**, 14.
- Larsell, O., Jansen, J., Korneliusson, H.K. & Mugnaini, E. (1972) *The Comparative Anatomy and Histology of the Cerebellum: The Human Cerebellum, Cerebellar Connections, and Cerebellar Cortex*. Minnesota Archive Editions, Oxford University Press, London.
- Magnotta, V.A., Gold, S., Andreasen, N.C., Ehrhardt, J.C. & Yuh, W.T. (2000) Visualization of subthalamic nuclei with cortex attenuated inversion recovery MR imaging. *NeuroImage*, **11**, 341–346.
- Mai, J.K., Paxinos, G. & Voss, T. (1997) *Atlas of the Human Brain*. Academic Press, San Diego.
- Massey, L.A., Miranda, M.A., Zrinzo, L., Al-Helli, O., Parkes, H.G., Thornton, J.S., So, P.-W., White, M.J., Mancini, L., Strand, C., Holton, J.L., Hariz, M.I., Lees, A.J., Revesz, T. & Yousry, T.A. (2012) High resolution MR anatomy of the subthalamic nucleus: imaging at 9.4 T with histological validation. *NeuroImage*, **59**, 2035–2044.
- Middleton, F.A. & Strick, P.L. (2000) Basal ganglia and cerebellar loops: motor and cognitive circuits. *Brain Res. Brain Res. Rev.*, **31**, 236–250.
- Morel, A. (2007) *Stereotactic Atlas of the Human Thalamus and Basal Ganglia*. Informa HealthCare USA, Inc., New York.
- Naidich, T.P., Duvernoy, H.M., Delman, B.N., Sorensen, A.G., Kollias, S.S. & Haacke, E.M. (2009) *Duvernoy's Atlas of the Human Brain Stem and Cerebellum*. Springer Verlag, Austria.
- Percheron, G., François, C., Talbi, B., Yelnik, J. & Fénelon, G. (1996) The primate motor thalamus. *Brain Res. Rev.*, **22**, 93–181.
- Reese, T.G., Heid, O., Weisskoff, R.M. & Wedeen, V.J. (2003) Reduction of eddy-current-induced distortion in diffusion MRI using a twice-refocused spin echo. *Magn. Reson. Med.*, **49**, 177–182.
- Sakai, S., Inase, M. & Tanji, J. (1996) Comparison of cerebellothalamic and pallidothalamic projections in the monkey (*Macaca fuscata*): a double anterograde labeling study. *J. Comp. Neurol.*, **368**, 215–228.
- Schäfer, A., Forstmann, B.U., Neumann, J., Wharton, S., Mietke, A., Bowtell, R. & Turner, R. (2011) Direct visualization of the subthalamic nucleus and its iron distribution using high-resolution susceptibility mapping. *Hum. Brain Mapp.*, **33**, 2831–2842.
- Schaltenbrand, G. & Wahren, W. (1977) *Atlas for Stereotaxy of the Human Brain*. Thieme, Stuttgart, pp. 84.
- Schmahmann, J.D., Doyon, J., McDonald, D., Holmes, C., Lavoie, K., Hurwitz, A.S., Kabani, N., Toga, A., Evans, A. & Petrides, M. (1999) Three-dimensional MRI atlas of the human cerebellum in proportional stereotaxic space. *NeuroImage*, **10**, 233–260.
- Seehaus, A.K., Roebroek, A., Chiry, O., Kim, D.-S., Ronen, I., Bratzke, H., Goebel, R. & Galuske, R.A.W. (2013) Histological validation of DW-MRI tractography in human postmortem tissue. *Cereb. Cortex*, **23**, 442–450.
- Stephan, K.E., Tittgemeyer, M., Knösche, T.R., Moran, R.J. & Friston, K.J. (2009) Tractography-based priors for dynamic causal models. *NeuroImage*, **47**, 1628–1638.
- Wiegell, M.R., Tuch, D.S., Larsson, H.B.W. & Wedeen, V.J. (2003) Automatic segmentation of thalamic nuclei from diffusion tensor magnetic resonance imaging. *NeuroImage*, **19**, 391–401.
- Wu, T. & Hallett, M. (2013) The cerebellum in Parkinson's disease. *Brain*, **136**(Pt 3), 696–709.
- Yelnik, J., Bardinet, E., Dormont, D., Malandain, G., Ourselin, S., Tandé, D., Karachi, C., Ayache, N., Cornu, P. & Agid, Y. (2007) A three-dimensional, histological and deformable atlas of the human basal ganglia. I. Atlas construction based on immunohistochemical and MRI data. *NeuroImage*, **34**, 618–638.